



Hydrogen production and simultaneous photoelectrocatalytic pollutant oxidation using a TiO₂/WO₃ nanostructured photoanode under visible light irradiation



T.T. Guaraldo^a, V.R. Gonçalves^b, B.F. Silva^a, S.I.C. de Torresi^b, M.V.B. Zanoni^{a,*}

^a Institute of Chemistry, São Paulo State University (UNESP), Rua Prof. Francisco Degni 55, 14800-900 Araraquara, SP, Brazil

^b Institute of Chemistry, São Paulo University (USP), Av. Prof. Lineu Prestes 748, Cidade Universitária, 05599-970 São Paulo, SP, Brazil

ARTICLE INFO

Article history:

Received 27 March 2015

Received in revised form 19 July 2015

Accepted 21 July 2015

Available online 3 August 2015

Keywords:

Bicomponent electrodes

TiO₂/WO₃ templates

Photoelectrochemical hydrogen production

Dye degradation

ABSTRACT

Photoelectrochemical (PEC) hydrogen production and simultaneous organic waste degradation is a re-emerging field. The main challenge of this technique has been the synthesis of new photoanode materials that are active towards visible light. Coupling close band gap energy oxides can be used to obtain materials with new optical and electronic properties. For this purpose, Ti/TiO₂/WO₃ electrodes were prepared by electrochemical anodization followed by templating and cathodic electrodeposition. The nanostructured bicomponent material was used as a photoanode for simultaneous hydrogen generation and organic dye degradation. A good photoactivity response (11 mA cm⁻²) was obtained under UV and visible light irradiation, when compared to pure TiO₂ (8 mA cm⁻²). Optimization of photoelectrochemical conditions revealed that pH optimization had a major impact on H₂ production, resulting in satisfactory hydrogen generation efficiency (46%) and dye removal (100% discoloration and 85% reduction in TOC). A dye oxidation mechanism is proposed, based on LC-MS/MS analyses. The TiO₂/WO₃ photoanode could potentially be used for environmental remediation and hydrogen generation under solar irradiation.

© 2015 Elsevier B.V. All rights reserved.

1. Introduction

The potential expansion of the use of TiO₂ as a semiconductor has been held back by its limited absorption in the ultraviolet region. Among the methods reported to produce photoactive TiO₂ in the visible light region, a promising strategy involves the coupling of semiconductor materials [1,2]. The coupling of two semiconductors presenting complementary optical properties can enhance electrode performance by improving charge separation (e⁻/h⁺), minimizing charge recombination, and increasing photoactivity [3]. The coupling of WO₃ and TiO₂ can be especially useful for the photoelectrocatalytic oxidation of organic species [4–9]. There are considerable benefits derived from the coupling of oxide materials containing close band gap energies, such as TiO₂ (3.2 eV) and WO₃ (2.8 eV). The valence and conduction band energy diagrams for WO₃ and TiO₂ bicomponent materials indicate electron injection from the TiO₂ conduction band to WO₃ is favored, while hole transfer between valence bands occurs in the opposite direction [4]. This can increase the number of holes across the TiO₂ surface and enhance the flow of electrons towards the counter electrode, kept under bias potential, hence improving photoelectrocatalysis efficiency. In addition, bicomponent films have shown greater photochemical activation than individual arrays of WO₃ or TiO₂ [4].

Most studies of TiO₂/WO₃ photoanodes have concerned coatings prepared by electrodeposition and electrosynthesis [8,10], while the preparation of templated TiO₂/WO₃ nanostructured films has received a reduced amount of attention [7]. Considering recent advances in photoelectrocatalysis is directly related to the morphologies of nanostructured semiconductors, the use of templates could offer a simple and versatile approach for the preparation of dimensionally controlled nanostructured TiO₂/WO₃ bicomponent films. Advantages of template synthesis include the ability to increase catalyst surface area, improve reaction/interaction between the semiconductor and the electrolyte, consequently enhancing charge transfer efficiency and reducing electron-hole recombination, and extend the absorption spectrum of the catalyst [3].

The cost of wastewater treatment is a major concern in industry, and there is a continual search for effective and inexpensive solutions. One attractive option is to employ photoelectrocatalytic techniques in order to explore a useful strategy by recovering the hydrogen generated at the counter electrode. In these methods, electrons are driven from the photoanode during the photoelectrocatalytic oxidation of organic compounds. Thus, in an ideal system, the organic pollutant is oxidized at the photoanode surface and photogenerated electrons move through an external circuit to the cathode, where reduction of protons occurs under anaerobic conditions. Therefore, the twin environmental benefits of waste material elimination and hydrogen generation could be an attractive way of adding value to wastewater treatment.

* Corresponding author.

E-mail address: boldrinv@iq.unesp.br (M.V.B. Zanoni).

In this work, we report the preparation of Ti/TiO₂/WO₃ bicomponent material by coating nanocavities with WO₃ film deposited by cathodic electrodeposition onto organized TiO₂ nanotube arrays obtained by electrochemical anodization. The aim was to enhance photoelectrocatalytic performance during irradiation from a commercial lamp that emitted UV and visible light. The photoanode was employed in the photoelectrocatalytic oxidation of Reactive Black 5 azo dye (RB5), used as an organic pollutant model, with simultaneous hydrogen generation at the Pt cathode. The dye oxidation was monitored together with the hydrogen production efficiency.

2. Experimental

2.1. TiO₂/WO₃ photoanode synthesis

The electrode materials were prepared following a sequence of four steps: TiO₂ nanotube formation, polystyrene templates self-assembly, WO₃ film formation, and templates removal. Titanium foils were submitted to a cleaning and polishing sequence, as described previously [7]. Formation of nanotubes was achieved by electrochemical anodization (30 V, 50 h) in 0.25 wt.% NH₄F in glycerol/water (90:10, v/v) [11]. The electrodes were fired at 450 °C for 30 min in a furnace (Model 650-14 Isotemp Programmable Muffle Furnace, Fisher Scientific).

In the next step, the surface was coated with monodispersed polystyrene nanoparticles used as templates (460 nm, Sigma Aldrich), diluted to 0.5% in 1.0×10^{-7} mol L⁻¹ Triton X-100, according to the procedure described previously [7,12]. Electrodeposition of the WO₃ film was performed at -0.45 V bias potential for 45 min [7,13]. The template was chemically removed under magnetic stirring in toluene (Synth) for 24 h. The electrode was then washed in Milli-Q water, dried in an N₂ atmosphere, and the WO₃ film was fired again at 450 °C for 30 min in a furnace.

The TiO₂/WO₃ bicomponent photoanode was compared to pure TiO₂ electrodes, where TiO₂ nanotubes were prepared by anodization according to the procedure described above [11].

2.2. Characterization of electrodes

All the synthesized electrodes were characterized by X-ray diffraction (XRD) using a Siemens D5000 X-ray diffractometer with Cu K α radiation, controlled using Diffrac Plus XRD Commander software. Morphological examination was performed by field emission gun scanning electron microscopy (FEG-SEM, EDS), using a JEOL 7500F microscope.

In order to evaluate the photocurrent response, linear scanning voltammograms were recorded in 0.1 mol L⁻¹ sodium sulfate solution in the range from -0.5 to 2.0 V, using a scan rate of 10 mV s⁻¹. The measurements were conducted in the absence and presence of irradiation from a commercial 125 W high-pressure mercury lamp (irradiance of 12.55 mW cm⁻²) with emission in the UV and visible regions [14].

2.3. Chemicals

Reactive Black 5 dye (55% purity) was purchased from Sigma Aldrich. This compound is used commercially as a textile dye. It is classified as harmful to humans according to US and EU legislation and its specifications are CAS 17095-24-8 and C.I. 20505. Dye solutions were prepared by direct dissolution of the powder in ultrapure water. All other reagents were used without previous treatment.

2.4. Photoelectrochemical reactor

All the photoelectrochemical measurements were performed in a PEC reactor consisting of two 25 mL compartments separated by a Nafion membrane and fitted with a quartz window (2.5 cm²) (Fig. 1). The PEC reactor was externally irradiated. All the experiments were

performed at room temperature (25 °C) using the previously prepared materials as working electrodes, Ag/AgCl as the reference electrode, and a Pt mesh as the counter electrode. The distance between the counter and working electrodes was 4.5 cm. All the photoelectrochemical measurements were carried out using an Autolab PGSTAT 302 potentiostat/galvanostat.

2.5. Hydrogen generation and dye degradation at TiO₂/WO₃ bicomponent, TiO₂, and WO₃ electrodes

Nitrogen was purged through the PEC reactor for 15 min prior to irradiation, in order to remove oxygen from the solution in each compartment. The amount of H₂ produced under irradiation was determined using a Thermo TRACE GC Ultra gas chromatograph equipped with TCD and FID detectors. A Carboxen-1006 PLOT column was used (30 m \times 0.53 mm) and the carrier gas was Ar at a flow rate of 60 mL min⁻¹. A 1 mL syringe was used for sample injection, and the oven, injector, and TCD temperatures were all kept at 150 °C. The analysis time was 8.5 min. Calibration curves were constructed using injection volumes of 20, 40, 60, 80, 100, 200, 300, 400, and 500 μ L. The hydrogen evolved was collected in an inverted burette.

The photoelectrochemical dye degradation was monitored by means of spectrophotometry (Model 8453, Hewlett-Packard), total organic carbon analysis (TOC-VCPN, Shimadzu, Japan), and high performance liquid chromatography (LC-MS/MS).

Prior to the chromatographic analysis, all the samples were submitted to solid phase extraction, using 3 mL Phenomenex cartridges, in order to remove the electrolyte from the degradation solutions. The extraction procedure used the following sequence: 3 mL methanol, 3 mL pure water, 500 μ L sample, 3 mL pure water, 2 mL ACN/MeOH (50:50), and 1 mL dichloromethane. After extraction, the samples were resuspended in water (150 μ L) before injection.

The analysis of the dye and its degradation products was performed by full scan enhanced mass spectrometry (EMS), with ion product analysis (EPI) for structural elucidation. Before injection, all samples were diluted in MeOH/H₂O (50:50, v/v) containing 0.1% formic acid. The analytes were separated on a Phenomenex Kinetex C-18 column (5 μ m, 150 mm \times 4.6 mm) coupled to an automatic injector (Model 1200, Agilent) and an HPLC pump (Model 1200, Agilent). Gradient mode was employed for the elution of byproducts, with 0.1% formic acid as a phase modifier in the eluent, over a period of 22 min. The solvents used were CH₃COONH₄ (50 mM in water) (A) and ACN (B), following the sequence: 90% A, 10% B (0–2 min); 100% B (2–17 min); 90% A, 10% B (17–22 min). The eluent flow rate was 1.0 mL min⁻¹ and the injection volume was 20 μ L.

The LC-MS/MS analysis was performed using a Model 1200 high performance liquid chromatograph (Agilent Technologies) coupled to a 3200 QTRAP quadrupole/linear ion trap mass spectrometer (AB Sciex Instruments) operated in negative ion mode with Turbolon Spray ionization. The spectral data were obtained at a vaporizer temperature of 550 °C, and nitrogen was used as the collision gas.

3. Results and discussion

3.1. Ti/TiO₂/WO₃ photoanode characterization

Fig. 2 shows the complete bicomponent electrode synthesis process and the FEG-SEM micrographs obtained for Ti/TiO₂/WO₃ photoanodes prepared using the electrochemical deposition and template method [7]. The image of the electrode prepared under optimized conditions (Fig. 2, image 2A) showed the surface completely covered by TiO₂ nanotubes 100 nm in diameter and with thickness of 30–40 μ m (measured by profilometry). The final electrodeposited WO₃ structure after template removal showed the presence of nanopores 500 nm in diameter and with thickness of 40–45 μ m (Fig. 2, image 2C). As previously reported [7], the XRD spectra (Fig. 2, images 3A and 3C) revealed diffraction

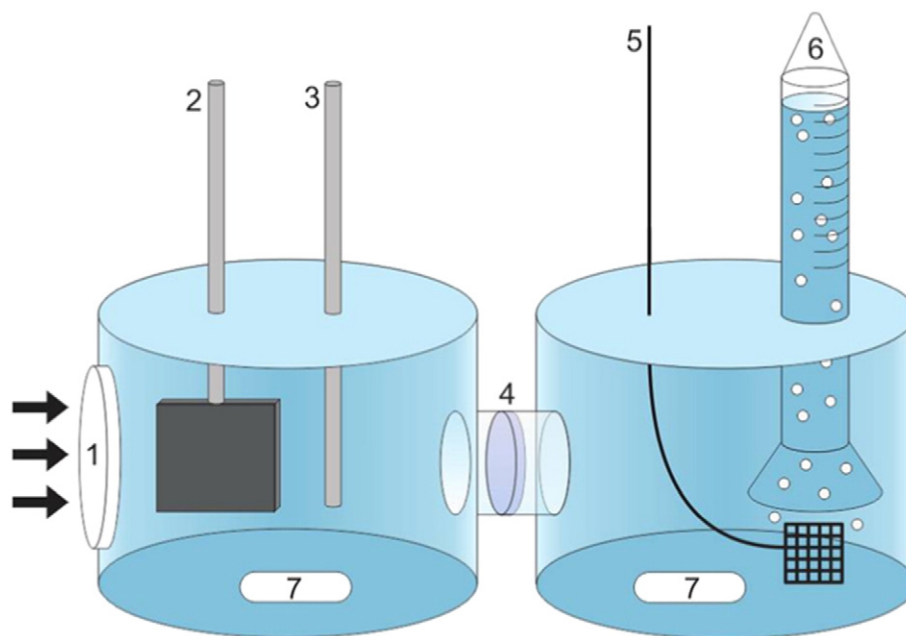


Fig. 1. Photoelectrochemical reactor used for dye degradation and hydrogen generation: (1) quartz window, (2) Ti/TiO₂/WO₃ working electrode, (3) Ag/AgCl reference electrode, (4) Nafion membrane, (5) Pt grid, (6) inverted gas burette, and (7) magnetic stirring.

peaks corresponding to TiO₂ anatase at $2\theta = 25$, Ti substrate at $2\theta = 40$, and an intermediate monoclinic W₁₈O₄₉ species at $2\theta = 20$. WO₃ in the monoclinic phase was identified by the presence of three peaks, at $2\theta = 23.06, 23.71, 24.36$ as well as three additional peaks at $33.16, 33.65,$ and 34.0 from tungsten trioxide phase. Energy dispersive X-ray spectroscopy (EDX) analysis (Fig. 2, image 3B) confirmed the presence of the main

elements composing the Ti/TiO₂/WO₃ electrode. The EDX spectrum displayed peaks with relative intensities typical of oxygen ($E = 0.5$ kV), titanium ($E = 4.5$ kV), and tungsten ($E = 1.7$ kV).

Fig. 3 compares photocurrent vs. potential curves obtained by recording linear sweep voltammograms using the Ti/TiO₂/WO₃ bicomponent electrode at 10 mV s^{-1} in $0.1 \text{ mol L}^{-1} \text{ Na}_2\text{SO}_4$, under dark

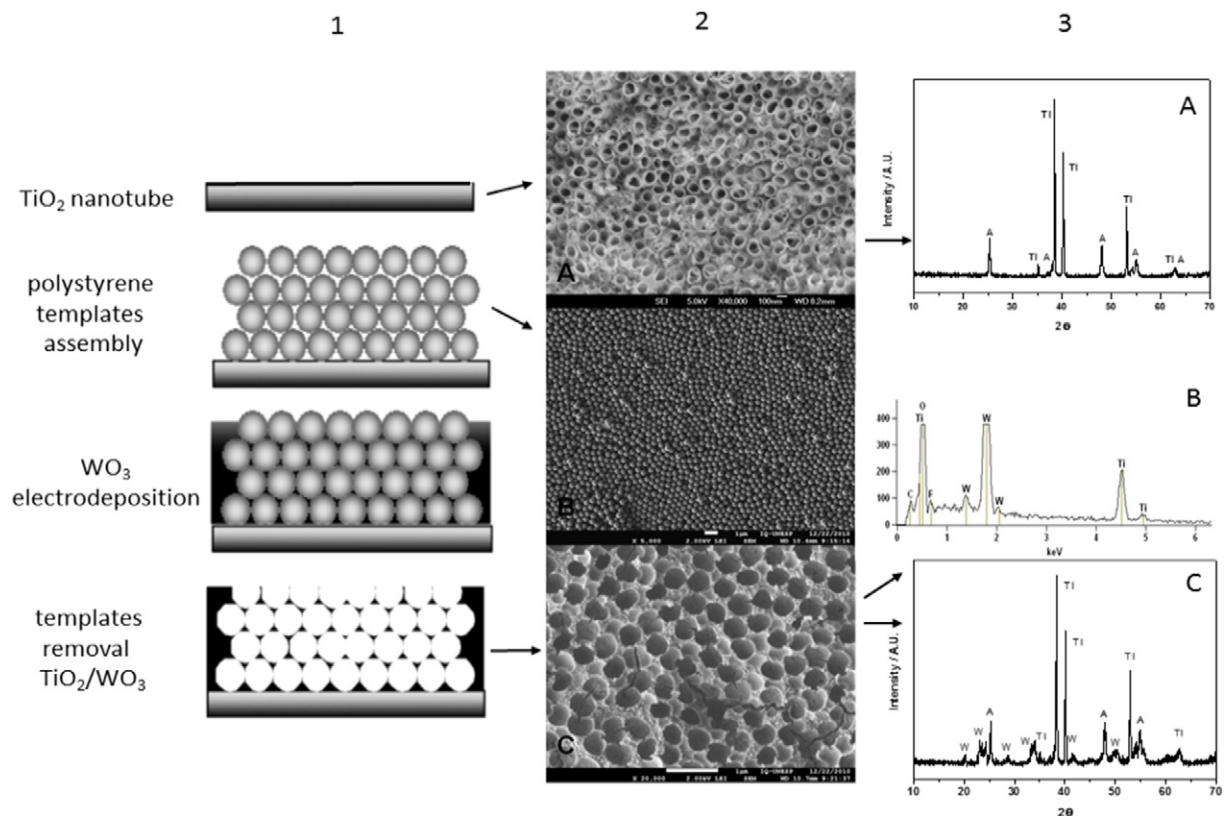


Fig. 2. (1) Ti/TiO₂/WO₃ template synthesis method, (2) FEG-SEM images, (3A and C) XRD analysis, and (3B) EDX analysis. Adapted from ref. 7).

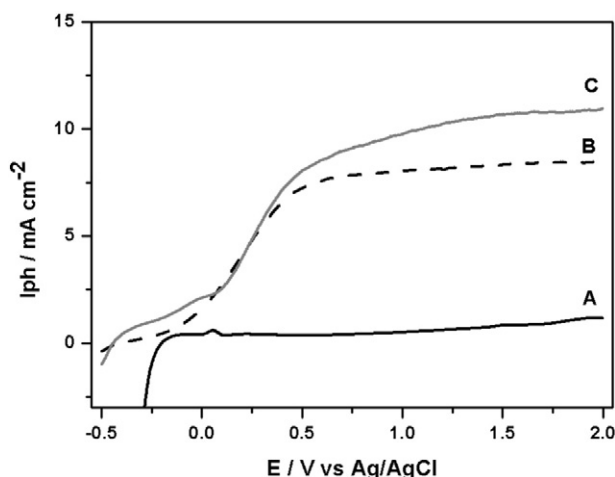


Fig. 3. Photocurrent-potential curves obtained in the range from -0.5 to 2.0 V, using a scan rate of 10 mV s⁻¹, for the Ti/TiO₂/WO₃ bicomponent nanostructured photoanode in the absence of light (A), and for the Ti/TiO₂ (B) and Ti/TiO₂/WO₃ (C) photoanodes irradiated by a commercial 125 W Hg lamp. The measurements were performed in 0.1 mol L⁻¹ Na₂SO₄.

conditions (curve A) and irradiated by UV-Vis light (curve C). For comparison, pure Ti/TiO₂ nanotubes voltammogram was also measured, without the WO₃ coating (curve B). The TiO₂/WO₃ bicomponent nanostructured photoanode exhibited a higher photocurrent response (11 mA cm⁻²), compared to the pure TiO₂ anode (8 mA cm⁻²). Both materials were photoactivated by light, because a fraction of the TiO₂ nanotubes was not coated by WO₃, due to the design of the template model for this bicomponent film. The photocurrent curve (curve C) shows contributions of both oxides; WO₃ was activated first (from -0.4 to 0.1 V), after which the TiO₂ contribution (from 0.1 V) can be observed. In the absence of irradiation, the photocurrent response was negligible for all the materials studied. The greater photoactivity of the bicomponent material could be attributed to the contributions of activation by the visible and UV light from the commercial lamp. The emission spectrum of the lamp showed greater intensity in the visible light region, at 435 , 550 , and 575 nm, compared to the UV region [14]. It was reported previously that TiO₂/WO₃ templated composites showed enhanced photoactivity, relative to a pure TiO₂ photoanode [4,15], and it is known that highly ordered and interconnected nanostructures favor electron transfer along the material [16].

3.2. Ti/TiO₂/WO₃ bicomponent electrode applied in degradation of Reactive Black 5 dye

Fig. 4 shows typical UV-Vis spectrum recorded for 5.0×10^{-5} mol L⁻¹ RB5 dye in 0.1 mol L⁻¹ Na₂SO₄ solution at pH 6.0 (curve A). The three main bands observed at 200 (3), 310 (2), and 600 nm (1) could be attributed to aromatic centers (2 and 3) and azo groups present in the molecule structure (1). The intensities of these bands decreased drastically after 20 min of photoelectrochemical treatment under $+1$ V potential applied to the Ti/TiO₂/WO₃ photoanode (curve C). Curve B shows the spectrum obtained for degradation performed with the TiO₂ electrode, and curve D shows the absorption spectrum of RB5 after 120 min of PEC treatment. Complete discoloration was obtained after both PEC treatments. The color removal constant rate followed pseudo-first order kinetics for both bicomponent (11.8×10^{-2} min⁻¹) and nanotube electrodes (10.6×10^{-2} min⁻¹). TOC removal obtained with the Ti/TiO₂/WO₃ electrode (85%) was around 12% higher than the TiO₂ electrode (73%). The increase in the degradation rate could be attributed to the different charge transfer in bicomponent materials, compared to charge mobility in pure oxides. The photogenerated electrons in the TiO₂ conduction band move

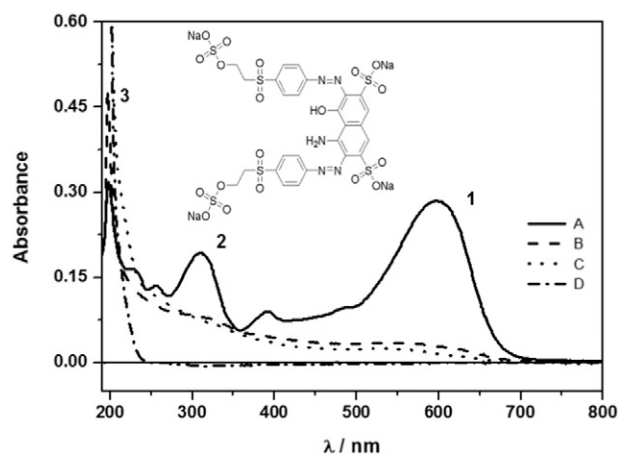
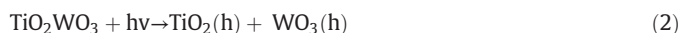
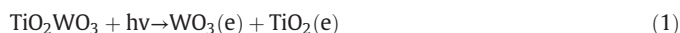
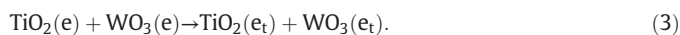


Fig. 4. Reactive Black 5 dye molecular structure and absorption spectrum in the UV-Vis region (A), comparative spectra for RB5 degradation using the TiO₂ (B) and TiO₂/WO₃ (C) photoanodes, and the spectrum obtained after 120 min of PEC treatment (D).

towards the WO₃ conduction band, due to the lower energy level. When holes move from WO₃ valence band towards TiO₂, they can become trapped on the TiO₂ surface leading to an increase in the recombination time. The photoelectrocatalytic efficiency of bicomponent material is therefore higher than that of TiO₂ [15]. It has been proposed that the charge transfer mechanism in TiO₂/WO₃ bicomponent electrodes involves the trapping of electrons from TiO₂ by hexavalent tungsten during the excitation process, with the tungsten being reduced to the pentavalent state (W⁵⁺) [17]. Oxygen then converts the pentavalent tungsten to the hexavalent state. These steps occur alongside formation of the hydroxyl radicals that participate in the degradation process. A schematic representation of the photoelectrocatalytic oxidation process at the TiO₂/WO₃ surface is provided in (Eqs. (1)–(7)) [18].



The photogenerated electrons are quickly trapped on the TiO₂ surface:



Electron pathway:



Hole pathway:



The photoelectrochemical behavior of the Ti/TiO₂/WO₃ bicomponent electrode is summarized in Fig. 5. Electrons and holes can be transferred from one to another semiconductor based on their conduction and valence band edge positions (E_{CB} and E_{VB}) [17]. The E_{CB} and E_{VB} values reported for WO₃ are $+0.25$ V and $+3.05$ V, respectively, while the corresponding values for TiO₂ are -0.2 V and $+3.2$ V [17]. Recombination is decreased with increased low band gap energy material. Upon irradiation, electrons of the composite material are excited from the valence band of both layers to the conduction band, leaving holes in the valence band. The photogenerated electrons of WO₃ are injected

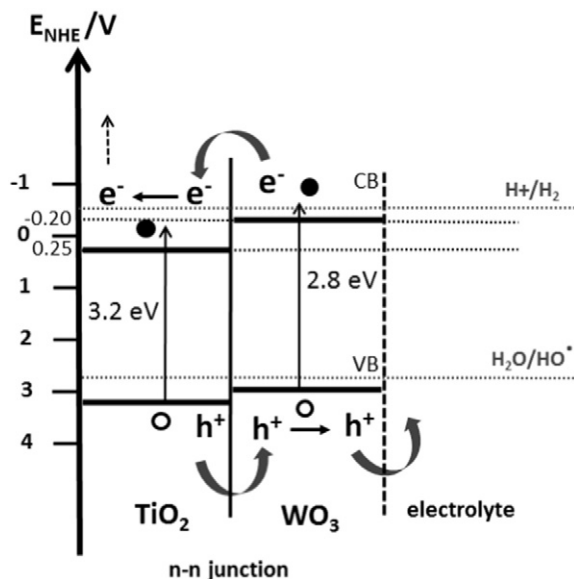


Fig. 5. Schematic representation of the photoelectrocatalytic mechanism for the TiO_2/WO_3 photoanode in contact with aqueous electrolyte at pH 7.

into the conduction band of TiO_2 , due to the heterojunction interface effect, easily reaching the substrate surface, and are transferred to the cathode via back contact, producing hydrogen [19,20]. Photogenerated holes, on the other hand, move into the WO_3 valence band in the opposite direction, driven by the built-in heterojunction field, and are finally carried out by the electrolyte to produce hydroxyl radicals at the photoanode in the photoelectrocatalytic reactor.

Fig. 6 compares dye degradation in the absence of applied potential (photocatalysis) and in the absence of catalyst (photolysis). These experiments were conducted in order to evaluate the contributions of the material (curve B), the applied potential (curve A), and the photolytic treatment with irradiation from the high-pressure mercury lamp (curve C). Dye degradation was monitored using UV–Vis spectrophotometry and TOC measurements.

The results demonstrated the dye color was easily removed in the presence of the bicomponent material (curve B) after 120 min of photocatalytic degradation, suggesting hydroxyl radicals could be responsible for breaking azo bonds, as one of the first steps of the oxidation process. The degradation kinetics was $4.9 \times 10^{-2} \text{ min}^{-1}$ and 48% mineralization was achieved. There was a lower influence of light on RB5 removal (curve C), with the photolytic treatment resulting in only 60% color

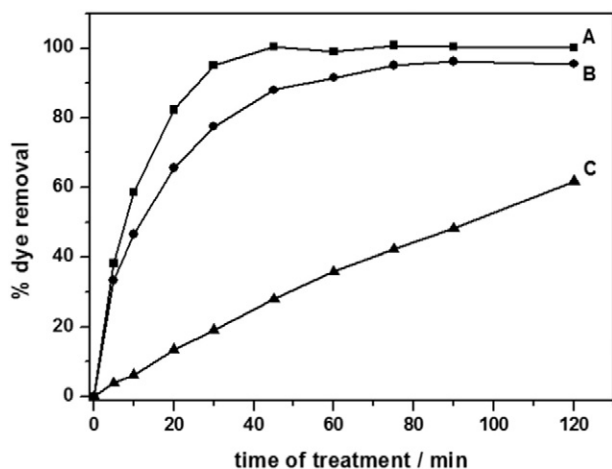


Fig. 6. RB5 dye degradation performed using different treatment techniques: photoelectrocatalysis (curve A), photocatalysis (curve B), and photolysis (curve C).

removal ($k = 1.55 \times 10^{-2} \text{ min}^{-1}$) and negligible mineralization. However, photoelectrocatalysis performed at +1.0 V with UV + Vis irradiation (curve A) increased the degradation rate to $11.8 \times 10^{-2} \text{ min}^{-1}$, indicating the large contribution of applied potential to the overall process.

3.3. LC-MS/MS analysis

Mass spectrometry analysis was used to evaluate the byproducts formed during the photoelectrocatalytic oxidation of RB5 dye, as well as the degradation pathway. Photoelectrochemical treatment of $7.0 \times 10^{-5} \text{ mol L}^{-1}$ RB5 dye in $0.1 \text{ mol L}^{-1} \text{ Na}_2\text{SO}_4$ at pH 6 (anodic compartment) and pH 4 (cathodic compartment) was performed for 150 min at +1.0 V using the $\text{Ti}/\text{TiO}_2/\text{WO}_3$ photoanode.

The RB5 dye chromatogram presented a peak at a retention time (t_r) around 8.0 min, detected as m/z 706 ($[\text{M}-2\text{H}_2\text{SO}_4]$), as shown in Fig. 9A. The identified ion for RB5 dye was different from the initial molecular mass (991 g mol^{-1}) of the dye structure. This could be attributed to the loss of four Na molecules, resulting in the hydrolyzed form ($899.82 \text{ g mol}^{-1}$). The dye structure is protonated in solution ($[\text{M}-4\text{Na} + 4\text{H}^+]$), with mass of 903 g mol^{-1} , and considering the negative mode ($[\text{M}-\text{H}]^-$), m/z is 902. The extracted ion chromatogram (XIC) for the RB5 dye is shown in Fig. 9A. The mass spectrum corresponding to the chromatographic band at 8.09 min (Fig. 9B) presented a peak at m/z 706, whose fragment ions spectrum is shown in Fig. 9C, and another signal at m/z 352 (Fig. 9B). The fragment ion spectrum of m/z 706 (Fig. 9C) showed two intense peaks at m/z 524.6 and 447.5, together with other less intense peaks at m/z 642.8, 511.5, 431.4, 344.5, and 278.5. This behavior has not been reported before in the literature, where mass spectrometric analysis has only been described for electrolytic [21] and biological [22] treatments.

The LC-MS/MS results obtained during the photoelectrochemical degradation of RB5 dye were used to track the presence of the dye peak at around 8.0 min. Complete peak area suppression was observed, confirming that treatment using TiO_2/WO_3 caused total removal of the dye, as found previously using UV–Vis spectrophotometric analysis. However, intermediate byproducts generated during dye degradation were identified at m/z 137, 183, 200, 210, and 280. Their chemical structures are shown in Table 2, together with the MS/MS product ions that confirmed their fragmentation. The concentrations of all the intermediates diminished as the treatment time increased. Three other ions, at m/z 248, 360, and 351, were rapidly formed and then completely degraded. The polar compounds with m/z 200 [22,23] and 183 [24] have already been reported. Based on the above results, it is

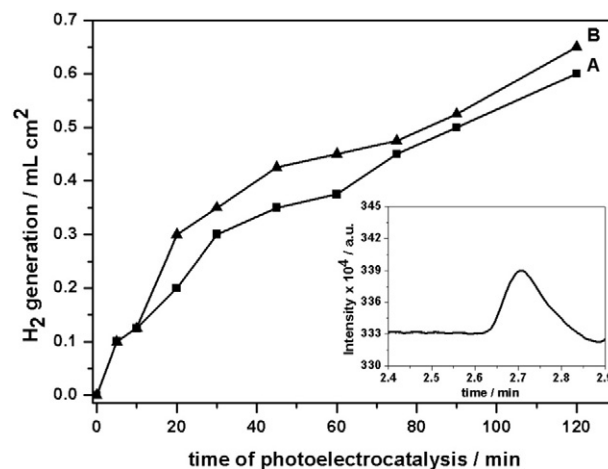


Fig. 7. Hydrogen volume generated during 120 min of photoelectrocatalytic oxidation of $1.0 \times 10^{-5} \text{ mol L}^{-1}$ RB5 dye under high-pressure mercury lamp irradiation in the presence of Ti/TiO_2 (A) and $\text{Ti}/\text{TiO}_2/\text{WO}_3$ (B) photoanodes. Inset: Chromatographic signal intensity of hydrogen ($t = 2.7 \text{ min}$) generated in the cathodic compartment.

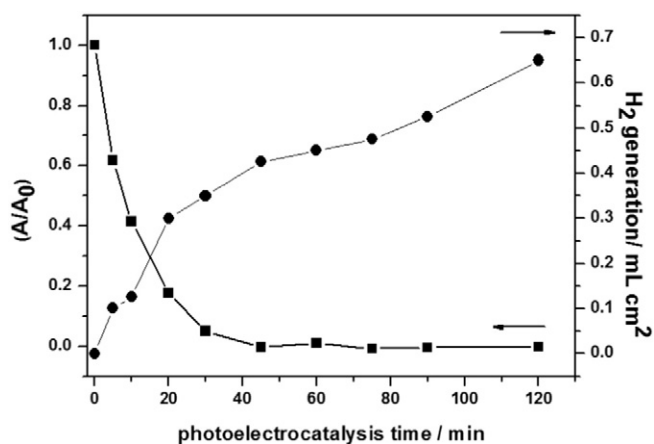


Fig. 8. Simultaneous hydrogen generation (•) and dye degradation (■) during photoelectrocatalytic oxidation of RB5 dye.

clear that RB5 dye was rapidly destroyed, mainly by means of hydroxyl radical oxidation on the bicomponent anode surface.

Considering the identified degradation byproducts, a degradation pathway involving parallel reactions is proposed, as shown in Fig. 10. The first step pathway is hydrolysis of the RB5 molecule, leading to m/z 742, followed by a catalytic elimination reaction due to NaOH addition, resulting in m/z 706. Next, m/z 706 undergoes a cyclization

reaction involving the $-NH_2$ and $-OH$ groups of the hydrolyzed RB5, yielding a $[M-2H]^{2-}$ ion with m/z 361.

In the next step of the sequence, hydroxyl radical-mediated desulfonation and hydroxylation generates m/z 436 and 200 ions. m/z 436 ion formation is also mediated by hydroxyl radical attack on the first azo bond, cleaving m/z 706 into m/z 436 and 200 ions, followed by subsequent reactions. The m/z 436 ion undergoes preferential attack of hydroxyl radicals on the second azo group, resulting in m/z 268. On the other hand, the m/z 200 ion loses one hydroxyl group, leading to m/z 183. The formation of alkylsulfonol phenolic compounds has been reported previously by Méndez-Martínez and collaborators [25]. The presence of byproducts detected even after 150 min of treatment indicates that recalcitrant material was obtained after 120 min of treatment.

3.4. Hydrogen generation

Experiments were carried out to measure the simultaneous generation of hydrogen at the cathode (Pt grid, area = 0.5 cm²). Fig. 7 illustrates the amount of hydrogen produced at the cathode during 120 min of photoelectrocatalytic oxidation of 1.0×10^{-5} mol L⁻¹ RB5 dye, under $E = 1.0$ V and UV + Vis irradiation of the Ti/TiO₂/WO₃ photoanode. The generation of hydrogen was confirmed by GC-TCD analysis, as shown in Fig. 7 inset. For comparison purposes, the results obtained using Ti/TiO₂ as the photoanode are also shown.

Hydrogen production in the cathodic compartment increased as a function of photoelectrolysis time, for all the photoanodes tested, but

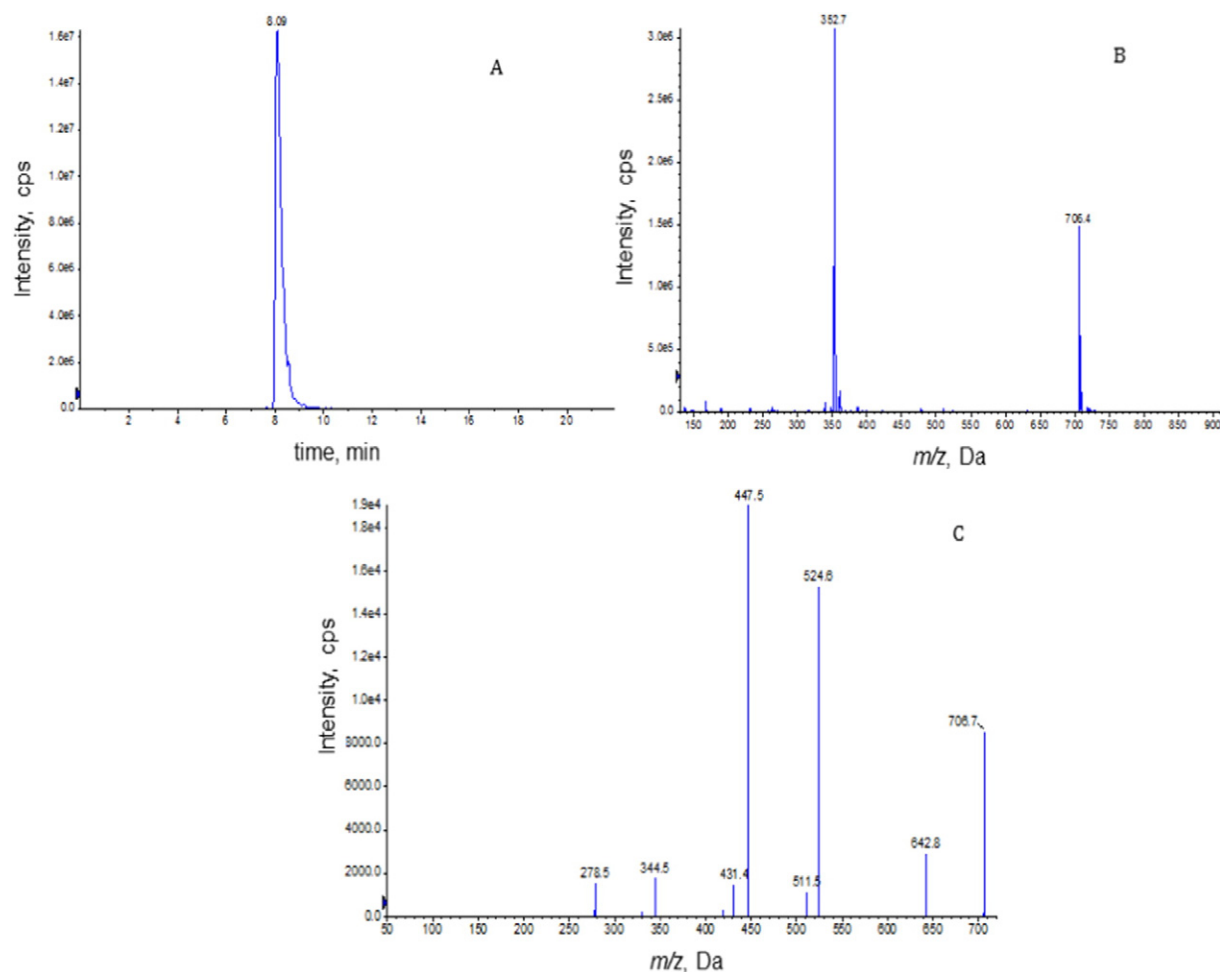


Fig. 9. Extracted chromatogram of the m/z 706 ion (A), mass spectrum of the chromatographic band at 8.09 min (B), and m/z 706 fragment ion spectrum (C).

Table 1

Dye discoloration, oxidation kinetics, TOC removal, volume of hydrogen, number of moles of hydrogen produced, and estimated hydrogen conversion efficiency for the degradation of $5.0 \times 10^{-5} \text{ mol L}^{-1}$ RB5 dye in $0.1 \text{ mol L}^{-1} \text{ Na}_2\text{SO}_4$ at 1 V potential using the bicomponent photoanode.

pH _{anode}	pH _{cathode}	% discoloration	k/min ⁻¹	% TOC removal	V _{H₂} (mL)	Moles of H ₂ produced	H ₂ estimated efficiency
2	4	100%	38.1×10^{-2}	95%	0.50	36.0×10^{-5}	15%
4	4	95%	12.5×10^{-2}	<50%	0.50	11.1×10^{-5}	30%
6	4	100%	11.8×10^{-2}	85%	0.65	5.0×10^{-5}	46%
8	4	85%	11.1×10^{-2}	<50%	1.00	4.2×10^{-5}	43%
10	4	90%	15.9×10^{-2}	<50%	0.50	5.6×10^{-5}	30%

was higher when the dye was oxidized at the bicomponent anode, compared to the pure TiO₂ anode. This indicated that there was an improvement in electron flow to the cathode when the photoelectrocatalysis of RB5 dye was performed using Ti/TiO₂/WO₃, confirming that the bicomponent anode amplified charge generation/separation.

In order to understand the formation of hydrogen in the coupled process, the photoelectrocatalytic oxidation of RB5 dye and hydrogen formation was carried out varying the pH in the cathode and anode compartments, the dye concentration, and the applied potential.

Alteration of the potential applied to the photoanode from 1.0 to 1.3 V decreased the efficiency of hydrogen production at the cathode by around 50%, although slightly higher RB5 dye discoloration was obtained at 1.3 V in the presence of the Ti/TiO₂/WO₃ photoanode. This behavior could be explained by the occurrence of water splitting at 1.23 V, which can be competitive with the water oxidation process on the photoanode [26]. At the same time, the increase in potential from 1.0 to 1.3 V led to a significant decrease in hydrogen generation efficiency, due to a decrease in the photoconversion efficiency of the Ti/TiO₂/WO₃ photoanode [15].

The influence of the pH in the anodic compartment, in the range of pH 2.0–10.0, was investigated for photoelectrochemical oxidation of

RB5 dye and concomitant hydrogen generation. The pH was kept constant during the degradations by correction with diluted solutions of H₂SO₄ and NaOH. In the cathodic compartment, the pH was initially adjusted to 4.0, and a pH of 2.0 was also tested. Table 1 shows the results obtained for dye discoloration, oxidation kinetics, and TOC removal during 120 min of photoelectrocatalysis at the Ti/TiO₂/WO₃ photoanode operated at 1 V, using $5.0 \times 10^{-5} \text{ mol L}^{-1}$ of RB5 dye in $0.1 \text{ mol L}^{-1} \text{ Na}_2\text{SO}_4$. Also shown in Table 1 are the numbers of moles of hydrogen formed and the estimated hydrogen conversion efficiencies at the pH values used.

Dye discoloration was observed at all pH values tested, but higher discoloration was obtained with pH 2 at the anode and pH 4 at the cathode. However, the minimum hydrogen generation efficiency was obtained under these conditions. As reported previously [27], hydrogen generation is favored when there is a pH gradient between the anodic and cathodic compartments. When the same acid pH is used in both compartments, a small amount of H₂ is produced. This is known as a chemically biased system [27]. If a pH difference is not maintained, both dye degradation and hydrogen evolution are impaired.

Hydrogen evolution and TOC removal were lower at acid pH values of 2 and 4 (anodic compartment). On the other hand, dye degradation was higher under these conditions. Similar mineralization was observed for pH values of 6, 8, and 10, although dye discoloration was lower than under acidic conditions, while hydrogen generation was increased. Reduction of the cathodic pH to 2.0 did not significantly improve hydrogen generation.

Under alkaline conditions, hydroxylated byproducts can be formed by reaction between dye degradation products and hydroxyl radicals present in the medium. These byproducts are more difficult to oxidize. Under acidic conditions, aliphatic short chain hydrocarbons are likely to be formed, which can be oxidized more easily, hence favoring discoloration.

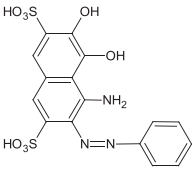
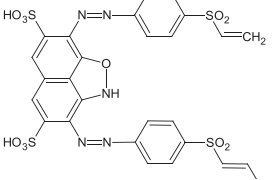
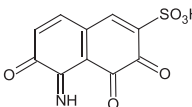
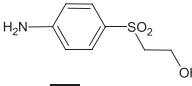
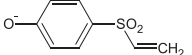
The results showed that the best experimental conditions for dye degradation and hydrogen evolution were pH 6 in the anodic compartment and pH 4 in the cathodic compartment. The nanostructured TiO₂/WO₃ bicomponent electrodes demonstrated efficient hydrogen generation, at a rate of $0.33 \text{ mL h}^{-1} \text{ cm}^{-2}$, corresponding to an estimated efficiency of around 46%.

3.5. Simultaneous dye degradation and hydrogen generation

Fig. 8 illustrates the performance of the system for simultaneous dye degradation and hydrogen generation during photoelectrocatalytic oxidation conducted with $1.0 \times 10^{-5} \text{ mol L}^{-1}$ of RB5 dye, using the Ti/TiO₂/WO₃ photoanode operated at 1 V bias potential under UV + Vis light. Complete dye degradation was obtained after 120 min of treatment, with 100% discoloration and around 85% TOC removal. There was concomitant formation of hydrogen, with a maximum of $5.0 \times 10^{-5} \text{ mol cm}^{-2}$ of hydrogen generated after 120 min of treatment, corresponding to 46% conversion efficiency. Table 3 shows a comparison of the charge consumed and the estimated hydrogen generation efficiency when the PEC treatment was performed with the TiO₂ anode. Lower charge consumption was observed for the Ti/TiO₂/WO₃ material, indicating that it could be an efficient means

Table 2

Byproducts identified during RB5 photoelectrocatalysis: proposed fragment ion structures, retention times, m/z ratios, and MS/MS product ions.

Proposed structure	(t _r)/min	[M-H] ⁻ or m/z	Productions MS/MS
	9.4	436	247.4 182.1
	7.9	361	247.2 216.0 182.1 164.0 80.4
Not identified	7.98	360	261.6 80.0
	6.4	248	233.9 221.2 150.3 80.0
Not identified	6.9	210	134.9 119.1
	10.5	200	184.2 170.1 156.1
	7.2	183	156.1 107.9 92.0

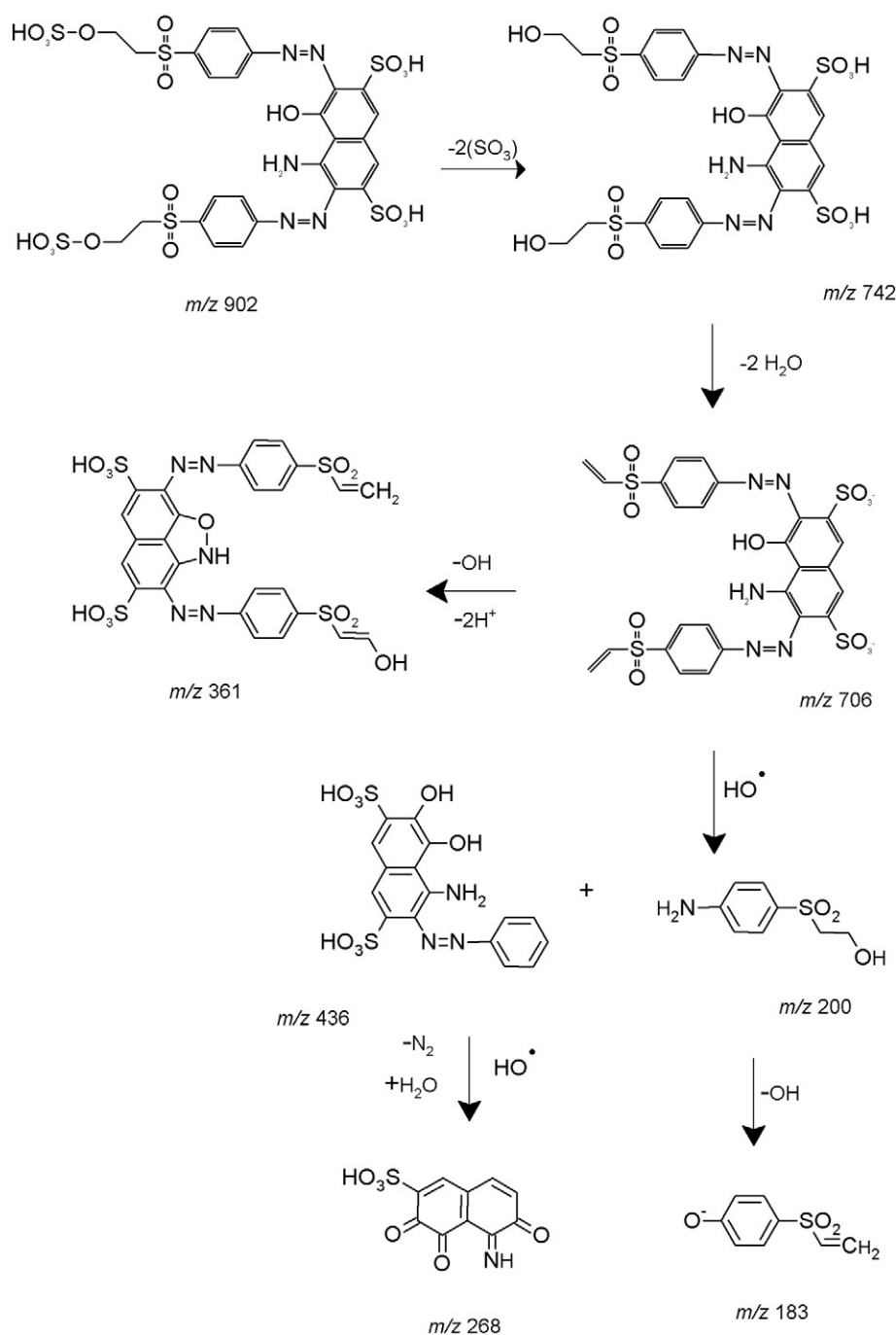


Fig. 10. Proposed degradation pathways for photoelectrocatalytic oxidation of RB5 dye.

of generating hydrogen as a renewable energy resource, while at the same time eliminating undesirable organic material.

4. Conclusions

A templating method was successfully used to synthesize a bicomponent electrode based on Ti/TiO₂/WO₃, where TiO₂ nanotubes were used as a platform for WO₃ deposition. The electrode could be photoactivated by visible and ultraviolet irradiation, and provided an enhanced photocurrent response, relative to plain Ti/TiO₂ electrode. The new material enabled more effective photoelectrocatalytic oxidation of Reactive Black 5 dye (RB5) under UV-Vis irradiation with an applied potential of +1 V, resulting in 100% discoloration and 85% TOC

removal after 120 min of treatment. LC-MS/MS analysis indicated the oxidation involved progressive degradation of the dye and formation of two main compounds as final products, with *m/z* of 268 and 183. Monitoring of simultaneous hydrogen generation due to electron flow to the cathode showed production of $5.0 \times 10^{-5} \text{ mol cm}^{-2}$ of the gas, using a two compartment reactor operated using $0.1 \text{ mol L}^{-1} \text{ Na}_2\text{SO}_4$, anode pH 6.0, cathode pH 4.0, +1.0 V bias potential, and UV + Vis irradiation.

The findings demonstrated that photoelectrocatalysis using the TiO₂/WO₃ bicomponent material as the photoanode provided faster dye degradation, greater mineralization, and improved hydrogen generation, compared to pure oxide electrode. Most of the byproducts formed from RB5 dye were consumed during the PEC

Table 3

Measured hydrogen volume, charge consumed, and estimated hydrogen generation efficiency after 120 min of photoelectrocatalysis of 1.0×10^{-5} mol L⁻¹ RB5 dye in 0.1 mol L⁻¹ Na₂SO₄ at +1 V potential for each photoanode studied.

Electrode	VH ₂ /mL	Consumed charge/C	H ₂ mols produced	Estimated H ₂ efficiency (%)
TiO ₂	0.60	10.80	5.6×10^{-5}	43
TiO ₂ /WO ₃	0.65	9.84	5.0×10^{-5}	46

treatment. Therefore, the proposed photoelectrochemical method using a bicomponent TiO₂/WO₃ electrode could be a promising alternative for both environmental remediation and energy generation under solar irradiation.

Acknowledgements

The authors thank FAPESP (process no. 2009/17346-1, 2008/10449-7, 2008/10449-7), CAPES, and CNPq (446245/2014-3) for financial support of this work. We are indebted to Dra. Sandra I. Maintinguer and Renan Pachiega of IQAr-UNESP for the GC-TCD analyses.

References

- M. Pelaez, N.T. Nolan, S.C. Pillai, et al., A review on the visible light active titanium dioxide photocatalysts for environmental applications, *Appl. Catal. B Environ.* 125 (2012) 331–349, <http://dx.doi.org/10.1016/j.apcatb.2012.05.036>.
- Y. Zhang, X. Xiong, Y. Han, et al., Photoelectrocatalytic degradation of recalcitrant organic pollutants using TiO₂ film electrodes: an overview, *Chemosphere* 88 (2) (2012) 145–154, <http://dx.doi.org/10.1016/j.chemosphere.2012.03.020>.
- G.G. Bessegato, T.T. Guaraldo, M.V.B. Zanoni, Enhancement of photoelectrocatalysis efficiency by using nanostructured electrodes, *Modern Electrochemical Methods in Nano, Surface and Corrosion Science/Intech* 2014, pp. 271–319, <http://dx.doi.org/10.5772/58333>.
- J. Georgieva, E. Valova, S. Armyanov, N. Philippidis, I. Poullos, S. Sotiropoulos, Bicomponent semiconductor oxide photoanodes for the photoelectrocatalytic oxidation of organic solutes and vapours: a short review with emphasis to TiO₂-WO₃ photoanodes, *J. Hazard. Mater.* 211–212 (2012) 30–46, <http://dx.doi.org/10.1016/j.jhazmat.2011.11.069>.
- J. Georgieva, S. Sotiropoulos, S. Armyanov, N. Philippidis, I. Poullos, Photoelectrocatalytic activity of bi-layer TiO₂/WO₃ coatings for the degradation of 4-chlorophenol: effect of morphology and catalyst loading, *J. Appl. Electrochem.* 41 (2) (2011) 173–181, <http://dx.doi.org/10.1007/s10800-010-0221-8>.
- E. Valova, J. Georgieva, S. Armyanov, et al., Morphology, structure and photoelectrocatalytic activity of TiO₂/WO₃ coatings obtained by pulsed electrodeposition onto stainless steel, *J. Electrochem. Soc.* 157 (5) (2010) D309–D315, <http://dx.doi.org/10.1149/1.3356001>.
- T.T. Guaraldo, T.B. Zanoni, S.I.C. de Torresi, et al., On the application of nanostructured electrodes prepared by Ti/TiO₂/WO₃ “template”: a case study of removing toxicity of indigo using visible irradiation, *Chemosphere* 91 (5) (2013) 586–593, <http://dx.doi.org/10.1016/j.chemosphere.2012.12.027>.
- J. Georgieva, S. Armyanov, E. Valova, I. Poullos, S. Sotiropoulos, Enhanced photocatalytic activity of electrosynthesised tungsten trioxide–titanium dioxide bi-layer coatings under ultraviolet and visible light illumination, *Electrochem. Commun.* 9 (3) (2007) 365–370, <http://dx.doi.org/10.1016/j.elecom.2006.09.028>.
- J. Georgieva, S. Armyanov, E. Valova, N. Philippidis, I. Poullos, S. Sotiropoulos, Photoelectrocatalytic activity of electrosynthesised tungsten trioxide–titanium dioxide bi-layer coatings for the photooxidation of organics, *J. Adv. Oxid. Technol.* 11 (2) (2008) 300–307.
- N. De Tacconi, C. Chenthamarakshan, K. Rajeshwar, T. Pauporte, D. Lincot, Pulsed electrodeposition of WO₃-TiO₂ composite films, *Electrochem. Commun.* 5 (3) (2003) 220–224, [http://dx.doi.org/10.1016/S1388-2481\(03\)00021-3](http://dx.doi.org/10.1016/S1388-2481(03)00021-3).
- J.C. Cardoso, T.M. Lizier, M.V.B. Zanoni, Highly ordered TiO₂ nanotube arrays and photoelectrocatalytic oxidation of aromatic amine, *Appl. Catal. B Environ.* 99 (1–2) (2010) 96–102, <http://dx.doi.org/10.1016/j.apcatb.2010.06.005>.
- V.R. Gonçalves, M.P. Massafra, T.M. Benedetti, D.G. Moore, S.I. Córdoba de Torresi, R.M. Torresi, Nanostructured thin films obtained by electrodeposition over a colloidal crystal template: applications in electrochemical devices, *J. Braz. Chem. Soc.* 20 (4) (2009) 663–673, <http://dx.doi.org/10.1590/S0103-50532009000400010>.
- J.R.C. Rocha, T.L. Ferreira, R.M. Torresi, M. Bertotti, An analytical application of the electrocatalysis of the iodate reduction at tungsten oxide films, *Talanta* 69 (1) (2006) 148–153, <http://dx.doi.org/10.1016/j.talanta.2005.09.010>.
- G.G. Bessegato, J.C. Cardoso, B.F. Da Silva, M.V.B. Zanoni, Enhanced photoabsorption properties of composites of Ti/TiO₂ nanotubes decorated by Sb₂S₃ and improvement of degradation of hair dye, *J. Photochem. Photobiol. A Chem.* 276 (2013) 96–103, <http://dx.doi.org/10.1016/j.jphotochem.2013.12.001>.
- K. Liu, Y.-C. Hsueh, C.-Y. Su, T. Perng, Photoelectrochemical application of mesoporous TiO₂/WO₃ nanohoneycomb prepared by sol-gel method, *Int. J. Hydrog. Energy* 38 (19) (2013) 7750–7755, <http://dx.doi.org/10.1016/j.ijhydene.2013.04.046>.
- E. Yang, J. Shi, H. Liang, W. Cheuk, Coaxial WO₃/TiO₂ nanotubes/nanorods with high visible light activity for the photodegradation of 2,3-dichlorophenol, *Chem. Eng. J.* 174 (2–3) (2011) 539–545, <http://dx.doi.org/10.1016/j.cej.2011.09.030>.
- S.A. Singh, G. Madras, Photocatalytic degradation with combustion synthesized WO₃ and WO₃/TiO₂ mixed oxides under UV and visible light, *Sep. Purif. Technol.* 105 (2013) 79–89, <http://dx.doi.org/10.1016/j.seppur.2012.12.010>.
- L. Yang, Y. Xiao, S. Liu, et al., Photocatalytic reduction of Cr(VI) on WO₃ doped long TiO₂ nanotube arrays in the presence of citric acid, *Appl. Catal. B Environ.* 94 (1–2) (2010) 142–149, <http://dx.doi.org/10.1016/j.apcatb.2009.11.002>.
- S. Choudhary, S. Upadhyay, P. Kumar, et al., Nanostructured bilayered thin films in photoelectrochemical water splitting – a review, *Int. J. Hydrog. Energy* 37 (24) (2012) 18713–18730, <http://dx.doi.org/10.1016/j.ijhydene.2012.10.028>.
- H. Zhang, G. Chen, D.W. Bahnemann, Photoelectrocatalytic materials for environmental applications, *J. Mater. Chem.* 19 (2009) 5089–5121, <http://dx.doi.org/10.1039/b821991e>.
- A.J. Méndez-Martínez, M.M. Dávila-Jiménez, O. Ornelas-Dávila, et al., Electrochemical reduction and oxidation pathways for Reactive Black 5 dye using nickel electrodes in divided and undivided cells, *Electrochim. Acta* 59 (2012) 140–149, <http://dx.doi.org/10.1016/j.electacta.2011.10.047>.
- X. Wang, X. Cheng, D. Sun, Interaction in anaerobic biodecolorization of mixed azo dyes of Acid Red 1 and Reactive Black 5 under batch and continuous conditions, *Colloids Surf. A Physicochem. Eng. Asp.* 379 (1–3) (2011) 127–135, <http://dx.doi.org/10.1016/j.colsurfa.2010.11.065>.
- X. Wang, X. Cheng, D. Sun, H. Qi, Biodecolorization and partial mineralization of Reactive Black 5 by a strain of *Rhodospseudomonas palustris*, *J. Environ. Sci.* 20 (10) (2008) 1218–1225, [http://dx.doi.org/10.1016/S1001-0742\(08\)62212-3](http://dx.doi.org/10.1016/S1001-0742(08)62212-3).
- A. Plum, A. Rehorek, Strategies for continuous on-line high performance liquid chromatography coupled with diode array detection and electrospray tandem mass spectrometry for process monitoring of sulphonated azo dyes and their intermediates in anaerobic–aerobic bioreactors, *J. Chromatogr. A* 1084 (1–2) (2005) 119–133, <http://dx.doi.org/10.1016/j.chroma.2005.03.001>.
- A.J. Méndez-Martínez, M.M. Dávila-Jiménez, O. Ornelas-Dávila, et al., Electrochemical reduction and oxidation pathways for Reactive Black 5 dye using nickel electrodes in divided and undivided cells, *Electrochim. Acta* 59 (2012) 140–149, <http://dx.doi.org/10.1016/j.electacta.2011.10.047>.
- Y. Xin, M. Gao, Y. Wang, D. Ma, Photoelectrocatalytic degradation of 4-nonylphenol in water with WO₃/TiO₂ nanotube array photoelectrodes, *Chem. Eng. J.* 242 (2014) 162–169, <http://dx.doi.org/10.1016/j.cej.2013.12.068>.
- L.J. Minggu, W.R. Wan Daud, M.B. Kassim, An overview of photocells and photoreactors for photoelectrochemical water splitting, *Int. J. Hydrog. Energy* 35 (11) (2010) 5233–5244, <http://dx.doi.org/10.1016/j.ijhydene.2010.02.133>.